Integrated_Supp_Figures, Tables, and Supp Notes

with all the changes highlighted in BLUE

for easy review

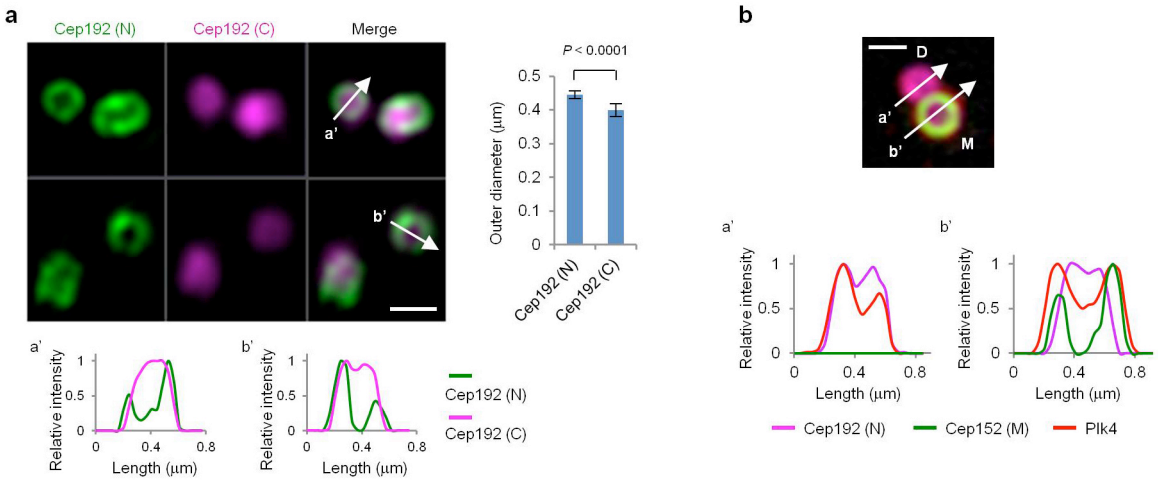

Supplementary Figure 1

Analyses of subcentrosomal localizations for Cep192, Cep152, and Plk4.

(**a**) U2OS cells immunostained with Alexa 488 (green)-conjugated Cep192 N-terminal (N) and Alexa 647 (magenta)-conjugated Cep192 C-terminal (C) antibodies were subjected to 3D-SIM microscopic analysis, as described in the Methods. Two representative images used for analyses were provided. The lines (a' and b') were drawn arbitrarily and their intensity line profiles (bottom left) were generated using the Zeiss ZEN software. The outer diameters of Cep192 (N) and (C) rings were quantified from G1 and S cells (n=44) (graph). Unevenly shaped toroids were excluded from quantification. Scale bars, 0.5 μm; error bars, s.d. (**b**) An example of measuring the diameter of Plk4 ring structure from either a daughter centriole without recruited Cep152 (a') or a mother centriole with already recruited Cep152 (b'). The image is from the **Figure 1a**, 1st panel. Cep192 ring structures were found to be associated with both mother and daughter centrioles at all times. The data quantified from the outer diameters of Plk4 rings are shown in **Figure 1b**. Scale bar, 0.5 μm.

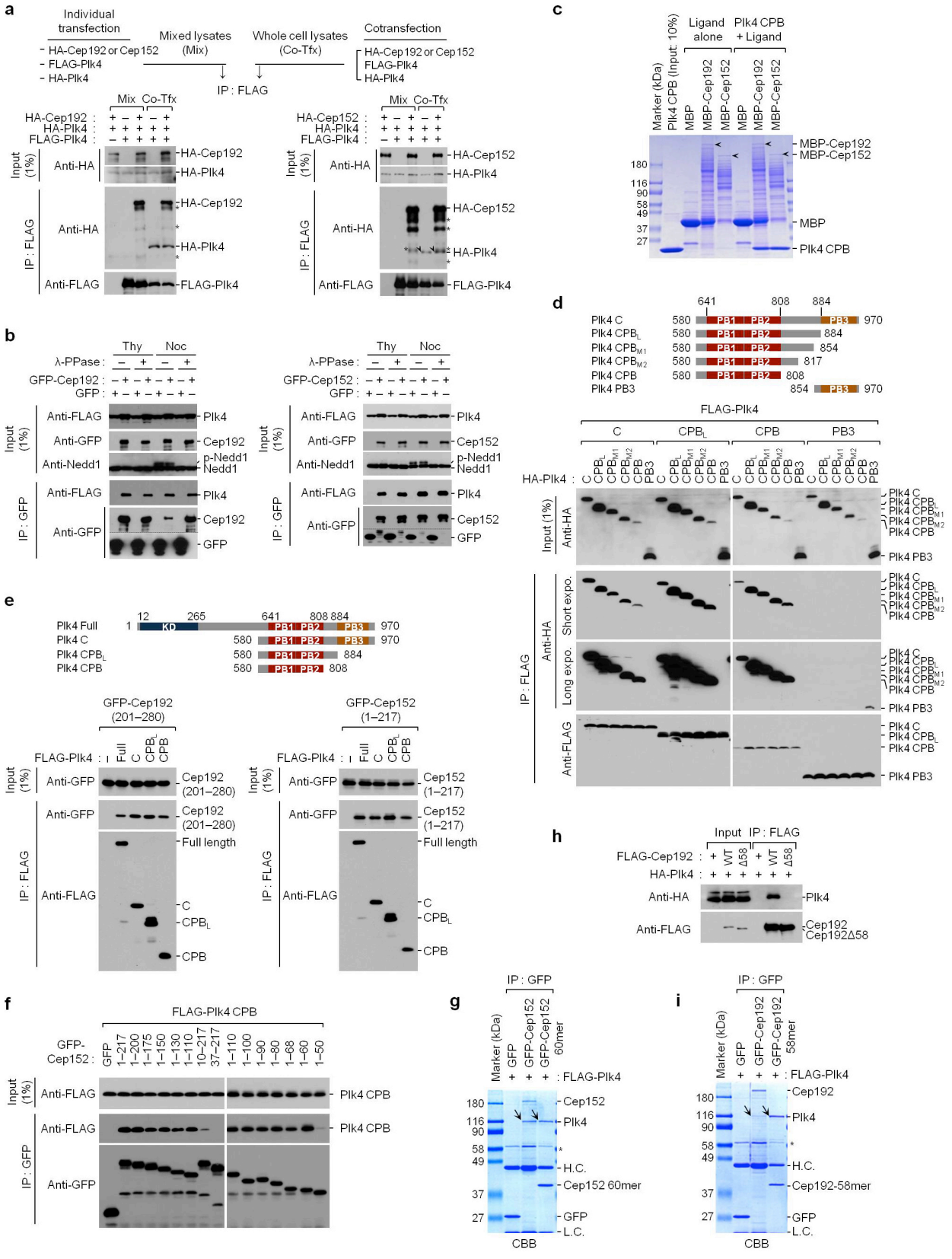
a
Individual transfection
Mixed lysates (Mix)
Whole cell lysates (Co-Tfx)
Cotransfection
HA-Cep192 or Cep152
FLAG-Plk4
HA-Plk4
IP : FLAG
Mix Co-Tfx
HA-Cep192 :
HA-Plk4 :
FLAG-Plk4 :
HA-Cep152 :
Input (1%)
IP : FLAG
Anti-HA
Anti-FLAG
b
Thy
Noc
λ-PPase :
GFP-Cep192 :
GFP-Cep152 :
GFP :
Anti-GFP
Anti-Nedd1
IP : GFP
Plk4
Cep192
Cep152
p-Nedd1
Nedd1
GFP
c
Marker (kDa)
Plk4 CPB (Input: 10%)
Ligand alone
Plk4 CPB + Ligand
MBP
MBP-Cep192
MBP-Cep152
Plk4 CPB
d
Plk4 C
Plk4 CPB$_L$
Plk4 CPB$_{M1}$
Plk4 CPB$_{M2}$
Plk4 CPB
Plk4 PB3
PB1 PB2 PB3
FLAG-Plk4
HA-Plk4 :
Input (1%)
IP : FLAG
Short expo.
Long expo.
e
Plk4 Full
KD
PB1 PB2 PB3
GFP-Cep192 (201–280)
GFP-Cep152 (1–217)
Full
Cep192 (201–280)
Cep152 (1–217)
Full length
f
FLAG-Plk4 CPB
GFP-Cep152 :
GFP
1–217
1–200
1–175
1–150
1–130
1–110
10–217
37–217
1–110
1–100
1–90
1–80
1–68
1–60
1–50
g
IP : GFP
GFP-Cep152
GFP-Cep152 60mer
FLAG-Plk4
Cep152
Plk4
H.C.
Cep152 60mer
GFP
L.C.
CBB
h
Input
IP : FLAG
FLAG-Cep192 :
WT
Δ58
Cep192
Cep192Δ58
i
GFP-Cep192
GFP-Cep192 58mer
Cep192
Cep192-58mer

Supplementary Figure 2

Human Plk4 CPB (580–808) fragment forms a stable homomeric complex and is sufficient to interact with Cep192 and Cep152 in a phospho-independent manner.

(**a**) A set of 293T cells was individually transfected with either HA-Cep192 (left) or HA-Cep152 (right), HA-Plk4, FLAG-Plk4, or control vector (–), where indicated, and the resulting lysates were mixed (Mix) prior to anti-Flag co-immunoprecipitation (IP) analysis. A second set of cells was co-transfected (co-Tfx) with the indicated constructs ("–" denotes empty vector) and the resulting lysates were subjected to anti-Flag co-immunoprecipitation analysis under the same conditions. Note that immunoprecipitation of FLAG-Plk4 co-precipitates HA-Plk4 under the co-transfected, but not mixed, conditions, suggesting that once a Plk4 homomeric complex is generated as Plk4 is expressed, it hardly exchanges its subunit with another molecule of Plk4. Asterisks, cross-reacting proteins with Cep192 or Cep152 immunoprecipitates; arrows, co-immunoprecipitated HA-Plk4 that migrates a little faster than a cross-reacting protein (asterisk). (**b**) 293T cells cotransfected with the indicated constructs were treated with thymidine (Thy) or nocodazole (Noc). The resulting lysates were incubated with either buffer alone (–) or λ-phosphatase (λ-PPase), and then subjected to co-immunoprecipitation (IP) analysis. Endogenous Nedd1, which is phosphorylated during mitosis [1], was immunoblotted to assess the efficiency of λ-phosphatase treatment under our experimental conditions. Note that λ-phosphatase treatment failed to alter the level of Plk4 interacting with Cep192 or Cep152. p-Nedd1, phosphorylated Nedd1. (**c**) MBP pull-downs were performed using bacterially expressed, purified proteins. Arrows indicate the full-length forms of MBP-fused Cep192 or Cep152. (**d**) 293T cells cotransfected with the indicated FLAG- or HA-tagged Plk4 constructs were subjected to immunoprecipitation (IP) analysis. Note that, when compared with other longer forms, the FLAG-Plk4 CPB (580–808) construct possessed the full capacity to interact with the Plk4 C-terminal region (C) (580–970) or other CPB variants. The PB3 (854–970), which is reported to form a homodimeric complex [2], showed a detectable level of interaction with another PB3 molecule only after a long exposure (expo.). (**e**) 293T cells cotransfected with various FLAG-Plk4 constructs and GFP-fused Cep192 (201–280) or Cep152 (1–217) [3] were subjected to immunoprecipitation (IP) analysis. (**f**) To determine the core region of Cep152 critically required for Plk4 CPB binding, 293T cells cotransfected with FLAG-Plk4 CPB (580–808) and various GFP-Cep152 (1–217) truncated forms were subjected to immunoprecipitation (IP) analysis. (**g**) 293T cells cotransfected with the indicated constructs were subjected to immunoprecipitation analysis. To achieve stable overexpression, a kinase-inactive Plk4 K41M mutant was used. The immunoprecipitates were analyzed by SDS-PAGE and stained with Coomassie (CBB). Arrows, coimmunoprecipitated FLAG-Plk4; Asterisk, cross-reacting protein; H.C., IgG heavy chain; L.C., IgG light chain. (**h**) 293T cells cotransfected with the indicated constructs were subjected to immunoprecipitation analysis. Δ58, Cep192 lacking residues 201–258. (**i**) 293T cells transfected with the indicated constructs were analyzed similarly as in (**g**). Arrows indicate FLAG-Plk4 coimmunoprecipitated with the GFP ligands. Asterisk, cross-reacting protein; H.C., IgG heavy chain; L.C., IgG light chain.

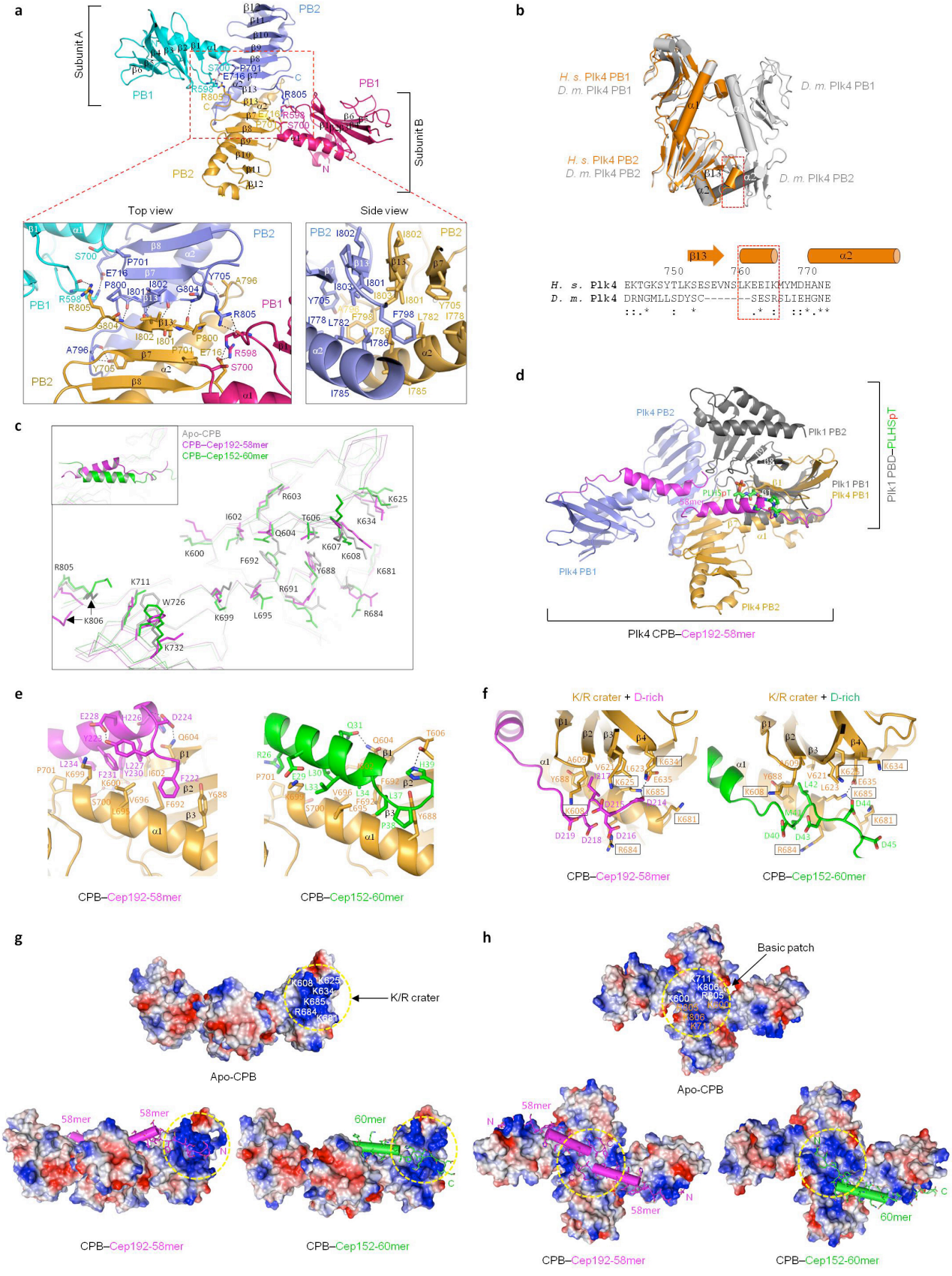
a
Subunit A
Subunit B
PB1
PB2
Top view
Side view
b
H. s. Plk4 PB1
D. m. Plk4 PB1
H. s. Plk4 PB2
D. m. Plk4 PB2
H. s. Plk4 EKTGKSYTLKSESEVNSLKEEIKMYMDHANE
D. m. Plk4 DRNGMLLSDYSC------SESRSLIEHGNE
c
Apo-CPB
CPB–Cep192-58mer
CPB–Cep152-60mer
d
Plk4 PB2
Plk1 PB2
Plk1 PB1
Plk4 PB1
Plk1 PBD–PLHSpT
Plk4 CPB–Cep192-58mer
e
CPB–Cep192-58mer
CPB–Cep152-60mer
f
K/R crater + D-rich
CPB–Cep192-58mer
CPB–Cep152-60mer
g
K/R crater
Apo-CPB
58mer
60mer
CPB–Cep192-58mer
CPB–Cep152-60mer
h
Basic patch
Apo-CPB
58mer
60mer
CPB–Cep192-58mer
CPB–Cep152-60mer

Supplementary Figure 3

The binding mode of the CPB–Cep192-58mer and the CPB–Cep152-60mer complexes.

(**a**) Analysis of the crystal structure of human apo-Plk4 CPB (PDB: 4N9J) revealed a dimeric interface formed between subunit A PB2 and subunit B PB2. The dimeric interface comprises four main chain hydrogen bonds (two reciprocal hydrogen bonds between the P800 of one subunit and the G804 of the other subunit, and a pair of hydrogen bonds between the two I802 residues from each subunit) (Top view), 2 additional hydrogen bonds between the Y705 of β7 and the A796 carbonyl of the α2-β13 loop (Top view), and multiple hydrophobic interactions (Y705, I778, L782, I785, I786, F798, I801, I802 and I803) between two β13 strands and also between two α2 helices (Side view). Within a subunit, the PB1 and PB2 domains are linked by evolutionarily conserved S700 and P701 residues. Remarkably, a pair of PB1-PB2 intersubunit hydrogen bonds is evident between the R598 carbonyl from the PB1 of subunit A and the R805 guanidyl from the PB2 of subunit B (Top view). These unique intersubunit interactions involving both PB1 and PB2 domains from two different subunits (i.e., subunit A and subunit B) may function like "a diagonal supporting beam of a triangular bracket" that stabilizes the "X-shaped" CPB structure by reinforcing not only the intersubunit PB2-PB2 junctional interaction but also the intrasubunit PB1-PB2 bridging (S700-P701) interaction. (**b**) Superposition of the structure of *Homo sapience* (*H. s.*) CPB (PDB: 4N9J) with that of *Drosophila melanogaster* (*D. m.*) CPB (PDB: 4G7N) revealed that an inserted sequence present in human Plk4 CPB clashed with the PB2 α2-helix of *Drosophila* CPB (red dotted box). The residues lacking in *Drosophila* CPB are indicated by dashed lines (bottom). The root-mean-square-deviation (r.m.s.d.) of superposed PB1-PB2 Cα atoms between human CPB (residues 586–807) and *Drosophila* CPB (residues 379–596) is 1.94 Å across 196 aligned residues (39.3% identity). Arrow and cylinder above the aligned sequences indicate β-strand and α-helix, respectively. Numbers indicate the positions of residues in the human Plk4 primary sequence. Identical residues are marked by '*'. Strongly conserved and weakly conserved residues are indicated by ':' and '.', respectively. The superposition was performed by using the *WinCoot*'s secondary structure matching program [4], and the sequence alignment was carried out using the *ClustalW2* program [5]. (**c**) The crystal structures of the CPB apo-form (gray) and the CPBs bound to Cep192-58mer (magenta) or Cep152-60mer (green) were superposed and shown as Cα traces. The CPB residues whose positions were greatly altered upon binding to Cep192-58mer or Cep152-60mer are indicated. The r.m.s.d. values for superposed PB1-PB2 Cα atoms of a subunit of the CPB dimer are 0.87 Å between apo-CPB and CPB-Cep192-58mer and 1.0 Å between apo-CPB and CPB-Cep152-60mer. Inset shows overall binding modes of the 58mer and the 60mer to CPB. (**d**) The crystal structure of the Plk4 CPB–Cep192-58mer complex was superposed with that of the Plk1 PBD–PLHSpT complex (PDB: 3HIK) [6]. Note that Plk1 PBD interacts with a phospho-peptide, PLHSpT, predominantly through the β1 of PB1 and the β8 and β9 of PB2 [6]. On the other hand, Plk4 CPB interacts with the 58mer peptide primarily through the α1 and β1 of PB1 and the β7 of PB2. The r.m.s.d. between Plk1 PB1 (residues 412–502) and Plk4 PB1 (residues 586–700) is 1.85 Å across 75 aligned residues (14.7% identity). (**e**) The interactions between CPB (orange) and the α-helical region of Cep192-58mer (magenta) and Cep152-60mer (green) are shown. Oxygen and nitrogen atoms are colored in red and blue, respectively. Hydrogen bonds important for the interaction are depicted as black dashed lines. In the case of the 58mer binding (left), the residues from its α-helix region were engaged in the hydrophobic interactions with the α1 and β1 of PB1 (i.e., the Y230 and L234 residues of the 58mer with the I602, K600 aliphatic portion, and P701 of the PB1, and the F222, Y223, L227, and F231 residues of the 58mer with the Y688, F692, L695, V696, and K699 aliphatic portion of the PB1). Additionally, the hydrogen bonds formed between the hydroxyl group of Y230 and the carbonyl of K600, and among D224, H226 (NH in the backbone), and Q604 residues stabilized the helical interactions. In the case of the 60mer binding (right), the residues from its α-helix were engaged in the multiple layers of well-arranged hydrophobic interactions with the residues from the CPB α1-helix, thus forming a highly stable antiparallel coiled-coil dimer between the two α-helices. The R26 aliphatic portion, L30, L33, L34, L37 and P38 from the 60mer formed prominent hydrophobic interactions with the K699 aliphatic portion, I602, V696, L695, F692, and Y688 (in order) from the α1-helix. Hydrogen bonds (Q31 with Q604 and H39 with T606) appeared to reinforce the multiple hydrophobic interactions formed between the two α-helices. (**f**) The interactions between CPB and the D-rich motif of Cep192-58mer (left) or Cep152-60mer (right) are depicted. Oxygen and nitrogen atoms are indicated in red and blue, respectively. The overall electron density was weak in this region to define specific interactions. The D-rich motifs of both Cep192-58mer and Cep152-60mer are surrounded by one arginine and five lysine residues (K608, K625, K634, K681, R684, and K685; rectangled in the figure), forming a crater-like structure. The three consecutive D214, D215, and D216 residues in the D-rich motif of the 58mer could engage in electrostatic interactions (dashed lines) with the K/R residues in the crater (D214 with K685 and D216 with R684) (left). In addition, the hydrophobic residue, I217, submerged (somewhat shallowly) into a hydrophobic pocket generated by the A609, V621, L623, K685 aliphatic portion, and Y688 from the PB1 of CPB. In the case of the 60mer, the D44 residue in the D-rich motif could be involved in an electrostatic interaction (dashed line) with K685 (right). This interaction was further stabilized by the L42 that was well embedded into the hydrophobic pocket at the center of the PB1 crater (right). (**g**,**h**) Surface representations of the overall structures of human apo-CPB (top) or CPB in complex with Cep192-58mer (left) or Cep152-60mer (right) are shown in both side (**g**) and top view (**h**). Surface colors represent electrostatic potentials depicted at the same scale (from −66.4 to +66.4) in all cases (red, negative; blue, positive; white, neutral). (**g**) In the apo-CPB, the K/R crater formed by surrounding one arginine and five lysine residues is indicated. The negatively charged residues from the 58mer D-rich motif appear to be effectively negated by the positive charged residues from the K/R crater. The binding of the 60mer modestly alters the electrostatic potential of the K/R crater, resulting in an enhanced exposure of nonpolar surface. Regardless of these changes, the D-rich motif-dependent interactions for both the 58mer and the 60mer are critically required for proper CPB binding (see **Figure 3c,d**). (**h**) In the apo-CPB, the presence of a basic patch (dotted circle) composed of six lysine and two arginine residues (symmetrically located pairs of K600, K711, R805, and K806 residues; the residues contributed from each subunit are colored in white or orange) is evident over the

dimeric interface. Unlike Cep192-58mer, Cep152-60mer possesses a unique N-terminal acidic sequence motif (residues from E15 to E21) that interacts with the basic patch residues by effectively neutralizing the electrostatic potential of this region. Binding of the 60mer altered the position of R805 and K806 present at the C-terminus of CPB (**Supplementary Figure 3c**). The positive dipole of the α-helix in the 60mer was also neutralized by the negatively charged side chains of its own. In contrast, the 58mer lacking an analogous acidic sequence failed to induce these effects. However, the neutralizing effect was in part achieved by the negative helical dipoles of two 58mer peptides aligned along the dimeric interface.

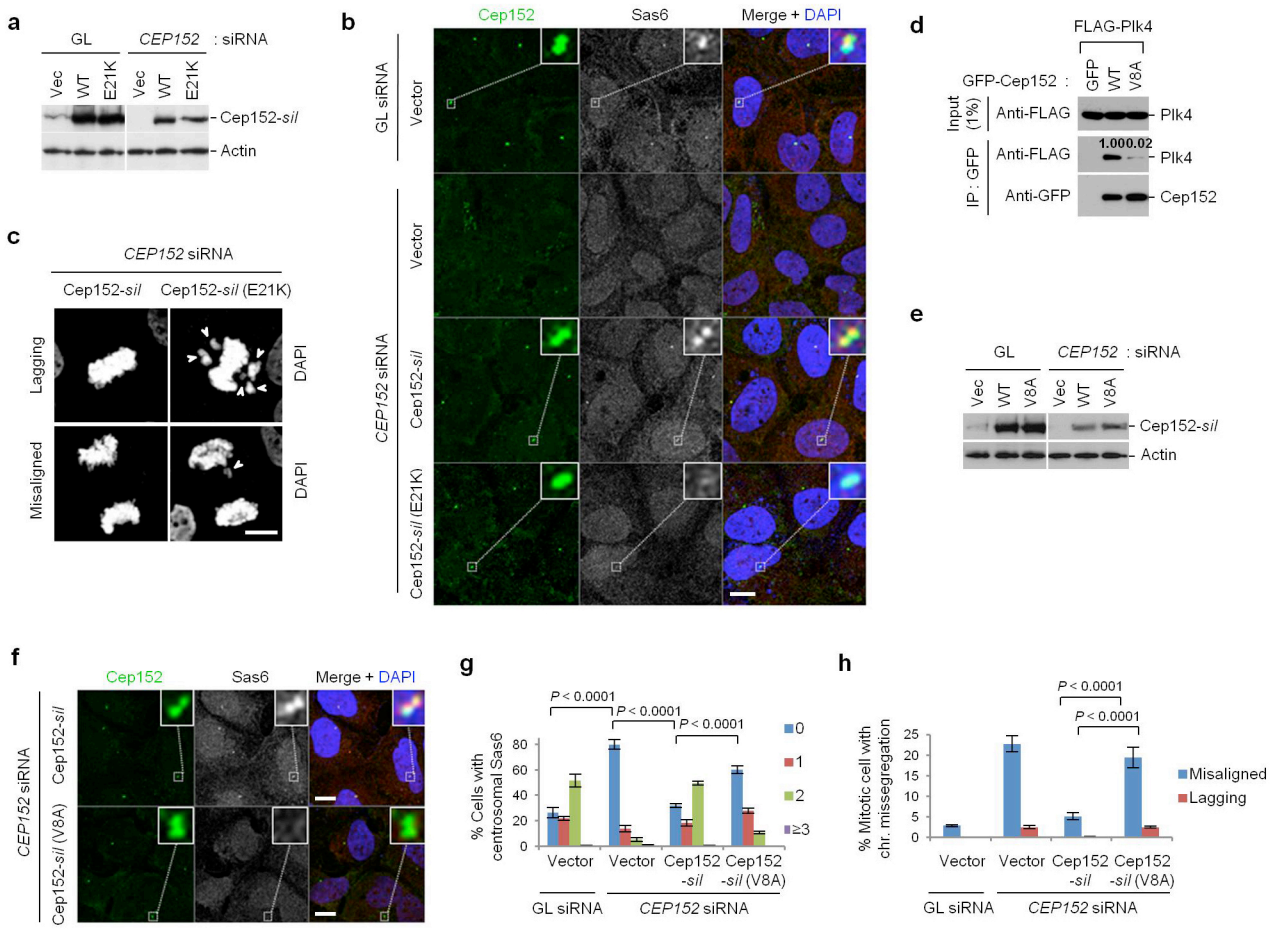

Supplementary Figure 4

Characterization of cancer-associated *CEP152 E21K* and *V8A* mutations impaired in Plk4 binding.

(**a–c**) The *CEP152 E21K* mutation found in human colon and rectum adenocarcinoma [Catalogue of Somatic Mutations in Cancer (http://www.sanger.ac.uk/ cosmic)] induces a defect in procentriole assembly. U2OS stably expressing either control vector or siRNA-resistant *CEP152-sil* or *CEP152-sil E21K* mutant (no tag) were silenced for either control *Luciferase* (GL siRNA) or *CEP152* (*CEP152* siRNA). (**a**) The resulting cells were subjected to immunoblotting analysis using the levels of actin as loading controls. (**b,c**) The cells in (**a**) were immunostained with anti-Cep152 and anti-Sas6 antibodies, and the fraction of interphase cells with centrosomally localized Sas6 (**b**) and the fraction of mitotic cells with abnormal (misaligned and lagging; arrows) chromosome morphologies (**c**) were quantified from three independent experiments. The results were provided in **Figure 3f,g**. Representative images used for quantification were shown. Scale bars in (**b,c**), 10 μm. (**d–h**) The *CEP152 V8A* mutation found in human ovarian serous cystadenocarcinoma [Catalogue of Somatic Mutations in Cancer (http://www.sanger.ac.uk/ cosmic)] induces a defect in procentriole assembly and chromosome segregation. (**d**) 293T cells cotransfected with the indicated constructs were subjected to immunoprecipitation (IP) analyses. Numbers, relative signal intensities. (**e**) U2OS stably expressing either control vector or siRNA-resistant *CEP152-sil* or *CEP152-sil V8A* mutant (no tag) were silenced for either control *Luciferase* (GL siRNA) or *CEP152* (*CEP152* siRNA), and then analyzed as in **Supplementary Figure 4a–c**. (**f**) The cells in (**e**) were immunostained with anti-Cep152 and anti-Sas6 antibodies. Representative images are shown. Scale bars, 10 μm. (**g,h**) From the samples obtained in (**f**), the number of centrosomal Sas6 signals (from 0 to ≥3) among interphase cells (**g**) and the number of mitotic cells with aberrant chromosomal morphologies (i.e., misaligned and lagging as shown in **Supplementary Figure 4a–c**) (**h**) were quantified from three independent experiments (≥200 cells/cell line/experiment). Bars, s.d.

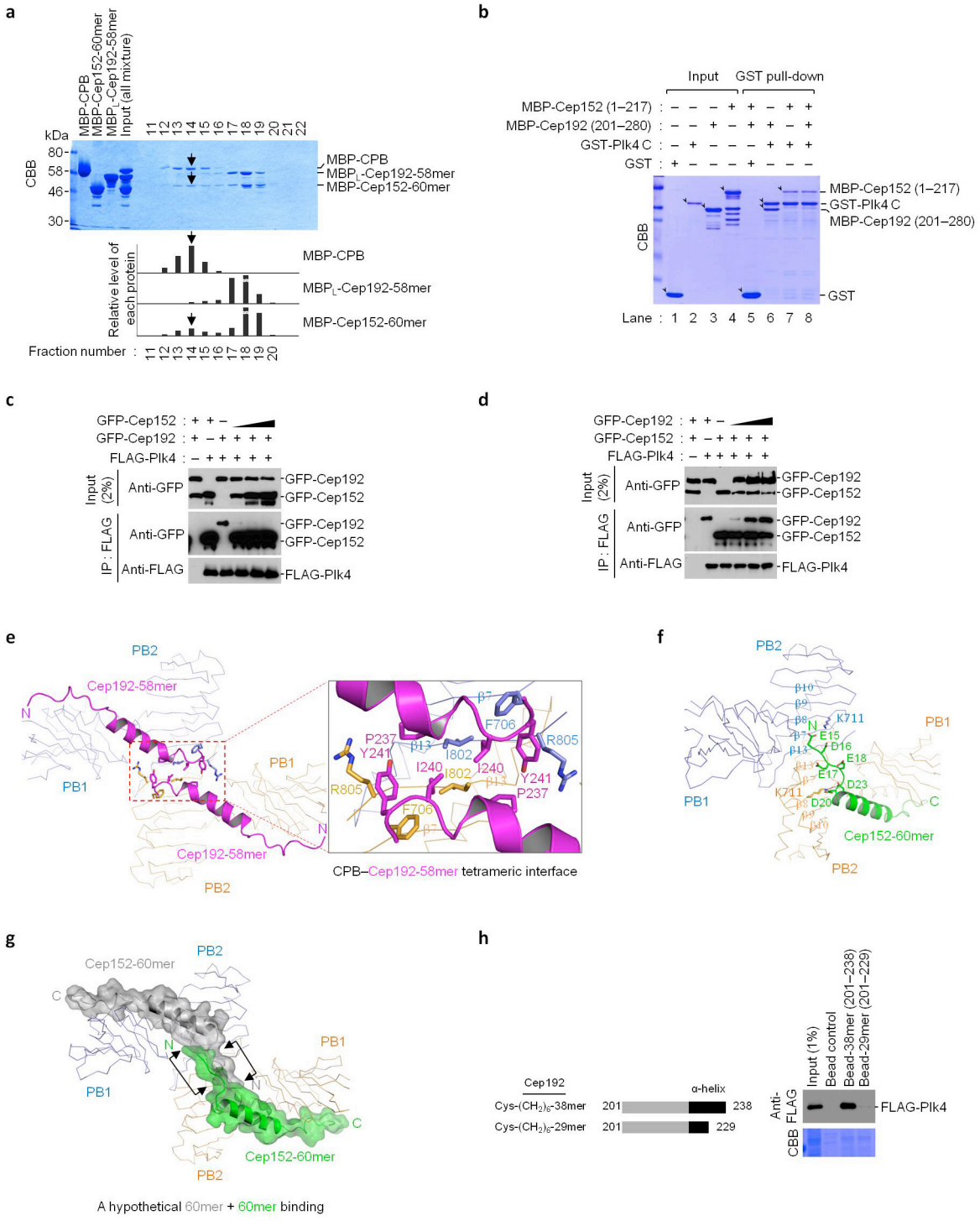

Supplementary Figure 5

The incompatible nature of Cep192-58mer and Cep152-60mer binding to Plk4 CPB.

(**a**) MBP-CPB, MBP-Cep152-60mer, and MBP$_L$-Cep192-58mer (MBP$_L$, a 30 residue-longer MBP variant, was needed to differentiate the size of MBP$_L$-Cep192-58mer from that of MBP-Cep152-60mer) were mixed and subjected to gel filtration chromatography.

Fractions were collected and analyzed by 10% SDS-PAGE. The gel was stained with Coomassie (CBB) and the proteins in each fraction were quantified (graphs). Arrows indicate the peak fraction (fraction #14) containing the highest amounts of the MBP-CPB–MBP-Cep152-60mer complex. Note that, unlike MBP-Cep152-60mer, MBP_L-Cep192-58mer hardly forms a complex with MBP-CPB. (**b**) To corroborate the incompatible nature of Cep192 and Cep152, we also used the two previously identified Plk4-binding fragments, Cep192 (201–280) and Cep152 (1–217) [3] (see **Supplementary Figure 2e**), expressed as MBP-fused forms, to carry out GST pull-downs with GST-Plk4 C-terminal (580–970) fragment (C). After incubating the purified proteins as indicated, bead-associated proteins were washed, separated by 10% SDS-PAGE, and stained with Coomassie (CBB). Arrowheads indicate full-length proteins with their expected sizes. Several cleavage products for Cep192 (201–280) and Cep152 (1–217) were evident. "–" indicates control buffer. Note that either Cep192 (201–280) or Cep152 (1–217) alone bound to Plk4 C efficiently (lanes 6 and 7). However, in the presence of both Cep192 (201–280) and Cep152 (1–217) in the same binding mix, the level of Cep152 (1–217) binding to the Plk4 C was unaffected, whereas that of Cep192 (201–280) binding to the Plk4 C was completely disrupted (lane 8). (**c,d**) 293T cells were singly transfected with either FLAG-Plk4, GFP-Cep192, or GFP-Cep152. Lysates were mixed in such a way that either GFP-Cep152 (**c**) or GFP-Cep192 (**d**) was gradually increased as indicated (black right-angled triangle). After immunoprecipitating FLAG-Plk4, coimmunoprecipitated Cep192 and Cep152 were analyzed. "–" indicates lysates transfected with control vector. Note that in the presence of equal amounts of Cep192 and Cep152 in the input, Cep152 outcompeted Cep192 in binding to Plk4 (the 4th lanes in **c** and **d**). When Cep192 was expressed several-fold higher than Cep152, Cep192 competitively bound to Plk4 at a level similar to that of Cep152 (the 6th lane in **d**). (**e**) The overall structure of the CPB–Cep192-58mer complex is shown with a close-up view of the tetrameric interface between the 58mer C-termini and the PB2-PB2 junction. Oxygen and nitrogen atoms are colored red and blue, respectively. The C-terminal regions of two 58mers bound to each subunit of the CPB dimer were arranged along the dimeric junction in reverse orientation, forming symmetrical hydrophobic interactions among P237, I240, and Y241 residues. In addition, the P237, I240, and Y241 residues also formed reciprocal hydrophobic interactions with I802, F706, and the R805 aliphatic portion from the β7 and β13 of PB2. These 58mer-58mer and 58mer-PB2 interactions may help promote the formation of the 2:2 CPB–58mer complex. (**f**) The 60mer binds to a CPB dimer in such a way that its N-terminal acidic residues (D20 and D23) interact with the K711 residue (orange) of a CPB subunit that it binds to (Cα trace in orange) and further extends toward the K711 residue (highlighted in blue) in the other subunit (Cα trace in blue). Since the K711 residue plays a critical role in binding to Cep152-60mer (see **Figure 3d**), the steric occlusion of the second K711 residue (blue) may prevent another 60mer from binding to the other CPB subunit. (**g**) In this hypothetical model, two 60mers bind to a CPB dimer, creating a steric clash (arrowed brackets) between the N-terminal regions of the two molecules. Therefore, this hypothetical tetrameric complex is not expected to exist *in vivo*. (**h**) 293T cells transfected with FLAG-Plk4 were incubated with control beads or bead-immobilized Cep192 38mer (201–238) or Cep192 29mer (201–229) peptides. Beads were precipitated and analyzed by immunoblotting analysis. The same membrane was stained with Coomassie (CBB). Note that the Cep192 (201–238) peptide containing both the D-rich motif and the α-helix motif efficiently precipitated Plk4. Under the same conditions, however, the Cep192 (201–229) peptide lacking a part of the α-helix failed to bind to Plk4. This result helps explain how a molecule of Cep152-60mer (surface representation in green in **Figure 4a**) bound to one of the two CPB subunits can effectively interfere with the α-helix motif-dependent interaction between the 58mer and the other subunit of the CPB dimer and prevent the 58mer from binding to this site.

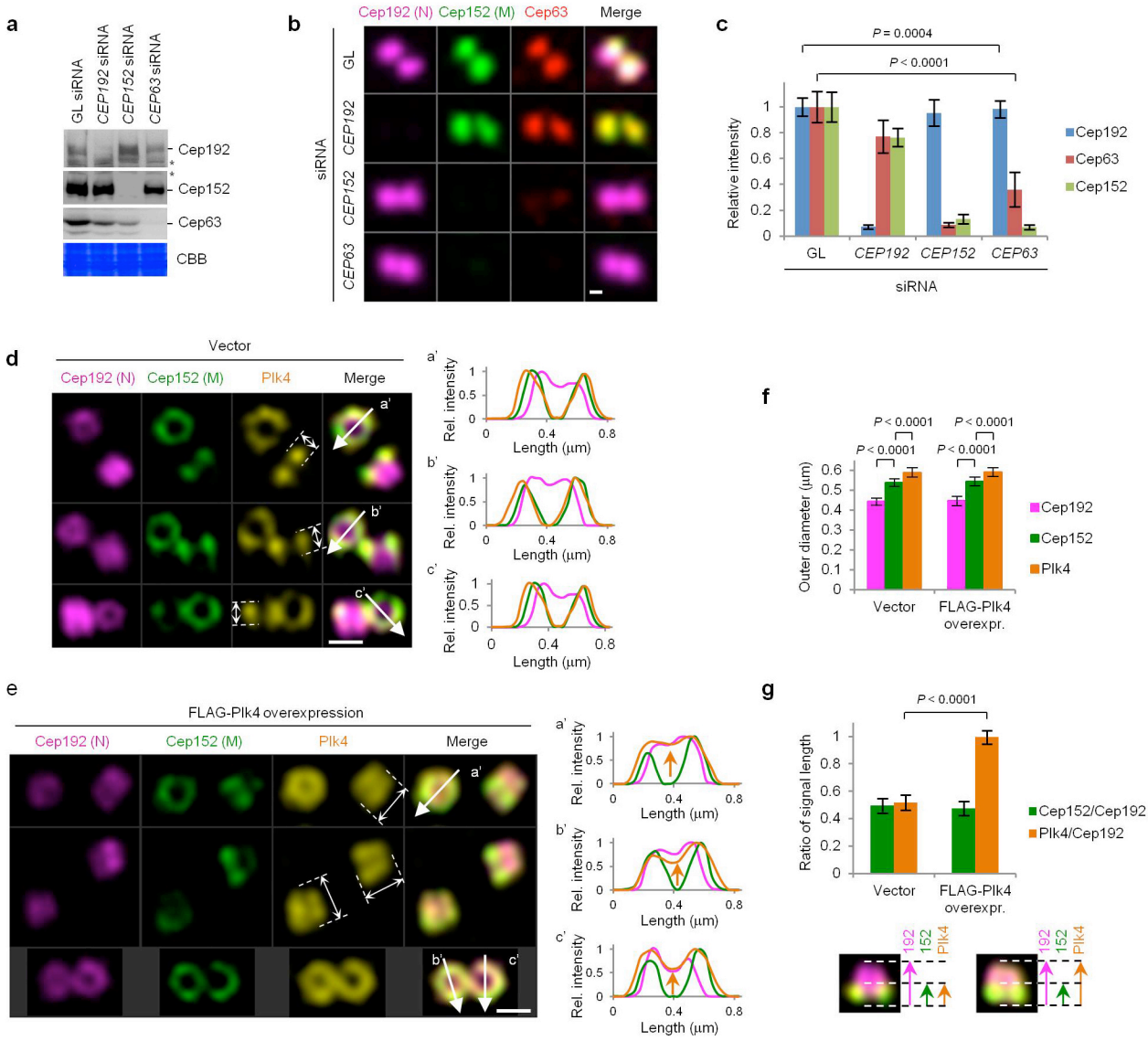

Supplementary Figure 6

Cep192 and Cep152 form two independent ring structures and overexpressed Plk4 localizes to the inner Cep192 ring even in the presence of the Cep152 ring.

(**a**) U2OS cells were silenced for control *Luciferase* (GL siRNA), *CEP192* (*CEP192* siRNA), *CEP152* (*CEP152* siRNA), or *CEP63* (*CEP63* siRNA) for 48 h. The resulting cells were harvested and subjected to immunoblotting analysis. Asterisk, cross-reacting protein; CBB, Coomassie-stained membrane. (**b,c**) The cells in (**a**) were immunostained with Alexa 647 (magenta)-conjugated anti-Cep192 N-terminal (N), Alexa 488 (green)-conjugated anti-Cep152 middle region (M), and anti-Cep63 (red) antibodies (**b**). The relative intensities of Cep192, Cep152, and Cep63 were quantified from three independent experiments (≥30 cells/cell line/experiment) (**c**). Scale bars in (**b**), 0.2 μm; error bars in (**c**), s.d. (**d,e**) hTERT-RPE cells infected with lentivirus expressing either control vector **(d)** or Flag-Plk4 **(e)** for 12 h were continuously cultured under serum starvation conditions for 36 h. The resulting cells were released into fresh medium for 3 h, fixed, and immunostained with anti-Plk4 (pseudo-colored in yellow), Alexa 647 (magenta)-conjugated anti-Cep192 (N) and Alexa 488 (green)-conjugated anti-Cep152 (M) antibodies. The samples were then subjected to 3D-SIM microscopic analysis as described in **Figure 1**. Experiments were performed in triplicates. Three representative images of each control vector **(d)**- and Flag-Plk4 **(e)**-expressing cell are shown. Scale bars, 0.5 μm. Two-sided double arrows with dotted lines indicate the length of the Plk4 signals along the longitudinal axes of the centrioles. Intensity line profiles are shown in (**d,e, right**). For all control vector-expressing cells (≥50 centrosomes/experiment), the Plk4 signal mirrored the Cep152 signal and was not detectable in the area of the Cep192 ring (**d**). In

contrast, cells overexpressing Flag-Plk4 exhibited greatly increased Plk4 signal at the Cep192-localized, inner regions of each cross-sectioned centrosome {upward pointing arrows in **(e)**}. In addition to the Plk4 signal present at the outskirts of the Cep152 rings, 137 out of 154 randomly selected centrosomes (~89%) displayed the inner Cep192-associated Plk4 signal, which was at least half the intensity of the main Plk4 peak at the outer Cep152 rings (i.e., ≥0.5 of the relative intensity shown in the graphs). Moreover, the Plk4 signal level at the inner centrosomal region was closely correlated with the Cep192 signal level, strongly suggesting that overexpressed Plk4 is recruited to the Cep192 ring structure. Consistent with this finding, Plk4 overexpression appeared to yield wider Plk4 fluorescent ring morphologies than control vector expression {compare the Plk4 ring thickness between (**d**) and (**e**)}. Rel. intensity, relative intensity. (**f**,**g**) Analysis of the images obtained in (**d**,**e**) revealed that the outer diameters of the Cep192, Cep152 and Plk4 rings in (**f**) were similar to those observed with U2OS cells in **Figure 1**. For the centrosomes with longitudinally placed centrioles, the lengths of Cep192, Cep152 and Plk4 signals along the longitudinal axes of the centrioles (see cartoon below the graph) and the ratios of their signal lengths (**g**) were calculated. Note that, while the length of endogenous Plk4 (~264 ± 26 nm) was similar to that of Cep152 (~259 ± 28 nm) and was about 50% of the length of the Cep192 (~525 ± 25 nm) in control cells, overexpressed Plk4 was detected along the entire length of Cep192-decorated centrioles. Error bars, s.d. from three independent experiments (≥50 centrosomes/cell line/experiment).

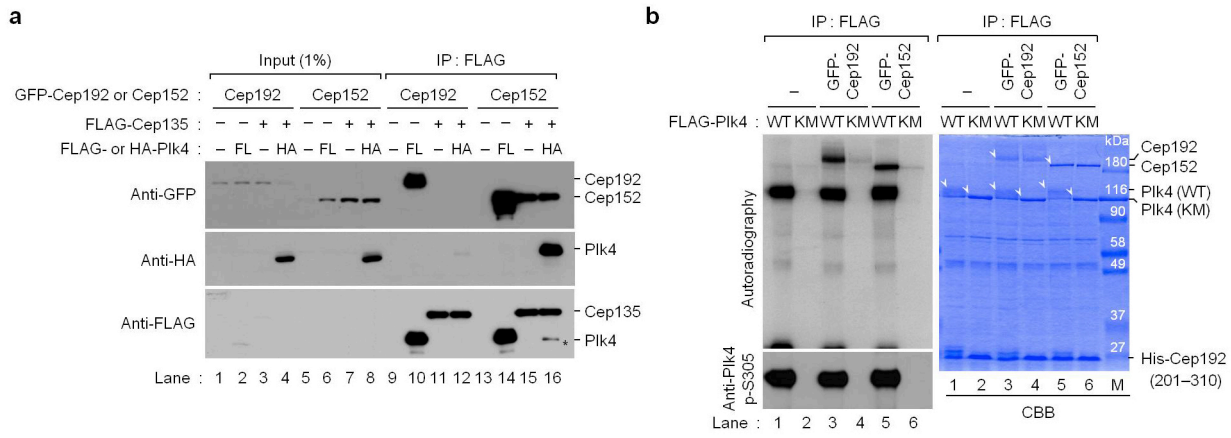

Supplementary Figure 7

The Cep152–Plk4 complex, but not the Cep192–Plk4 complex, binds to Cep135 without altering Plk4 kinase activity.

(**a**) Immunoprecipitation of Cep135 from transfected 293T cells coprecipitated Cep152, but not Cep192 (compare lane 15 with lane 11). A significant level of Plk4 was also present in the Cep135 immunoprecipitates (lane 16). HA, HA-tagged Plk4; FL, FLAG–tagged Plk4; asterisk, a signal stemming from the second anti-HA blot. "–" indicates control vector transfection. (**b**) Anti-FLAG immunoprecipitates prepared from transfected 293T cells (see the Methods) were subjected to immunocomplex kinase assays using His_6-Cep192 (201–310) as an *in vitro* substrate. The resulting samples were analyzed by both autoradiography and immunoblotting analysis with an anti-Plk4 p-S305 antibody. The level of the p-S305 epitope serves as a marker for Plk4 activity [7]. "–" indicates control vector-transfected cells. Note that Plk4 WT, but not the kinase-inactive K41M mutant (KM), phosphorylated coimmunoprecipitated Cep192 and Cep152 efficiently (compare lanes 3 and 5 with lanes 4 and 6), suggesting that Cep192 and Cep152 are Plk4 substrates *in vivo*. Arrowheads indicate the respective proteins. Numbers in the M lane, molecular weights (kDa) for the size markers.

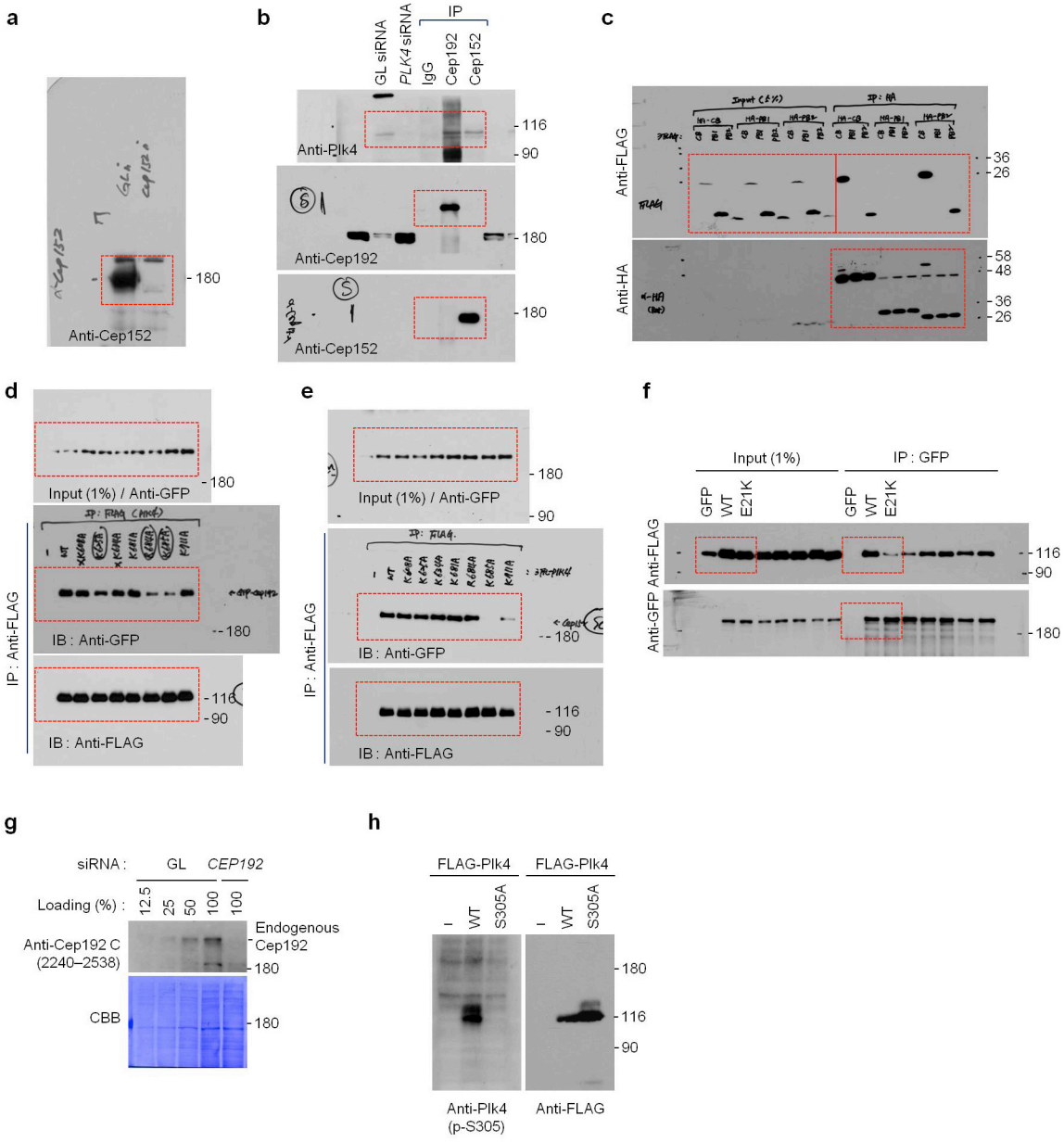

Supplementary Figure 8

Uncropped immunoblot images for the main figures and antibody validation results.

(**a**) Related to **Figure 1c**, (**b**) Related to **Figure 2a**, (**c**) Related to **Figure 2b**, (**d**) Related to **Figure 3c**, (**e**) Related to **Figure 3d**, (**f**) Related to **Figure 3e**, (**g**) Related to **Supplementary Figure 1** that used an anti-Cep192 C (2240–2538) antibody, and (**h**) Related to **Supplementary Figure 7** that used an anti-Plk4 p-S305 antibody.

Supplementary Table 1. Antibodies used in this study

Antibodies	Species	Cat #	Source	Exp. dilutions
Anti-Cep192 N (1–500)	Rabbit		Ref. 3	1:1000 (IB), 1:100 (IF), 5 μg (IP)
Anti-Cep192 C (2240–2538)	Rabbit		This study	1:1000 (IB), 1:100 (IF), 5 μg (IP)
Anti-Cep152 M (491–810)	Rabbit		Ref. 3	1:1000 (IB), 1:100 (IF), 5 μg (IP)
Anti-Plk4 (580–970)	Rabbit		Ref. 3	1:1000 (IB), 1:100 (IF)
Anti-Plk4 p-S305	Rabbit		This study	1:1000 (IB)
Anti-Sas6	Mouse	sc-81431	Santa Cruz	1:100 (IF)
Anti-GFP	Rabbit	sc-8334	Santa Cruz	1:1000 (IB), 2 μg (IP)
Anti-FLAG (clone M2)	Mouse	F1804	Sigma	1:1000 (IB), 2 μg (IP)
Anti-HA (clone 3F10)	Rat	11867423001	Roche	1:1000 (IB), 2 μg (IP)
Anti-Nedd1	Rabbit		Ref. 1	1:1000 (IB)
Anti-Actin	Rabbit	A2066	Sigma	1:1000 (IB)
Anti-Cep63	Rabbit	06-1209	Millipore	1:1000 (IB)

Supplementary Table 2. siRNA sequences used in this study

Target gene	Sequence (nt positions from the start codon)	Source	Type
Luciferase	CGTACGCGGAATACTTCGA	Ref. 8	Synthetic
CEP192	GCTAGTATGTCTGATACTTGG (2407–2427)	Ref. 9	Synthetic
CEP152	GCGGATCCAACTGGAAATCTA (3099–4019)	Ref. 9	Synthetic
CEP63	GGAGCTCATGAAACAGATT	Ref. 10	Synthetic

Supplementary Notes

Plasmid construction

FLAG-tagged constructs containing the full length wild-type (WT) (pKM3445), the full-length K41M kinase-inactive mutant (pKM3488), C (pKM3507), CPB_L (pKM3508), CPB (pKM3674), PB1 (pKM4337), PB2 (pKM4338), or PB3 (pKM3675) of Plk4 were generated by inserting each respective *Pme*I-*Not*I fragment into the pCI-neo-FLAG vector digested by the corresponding enzymes. All the FLAG epitopes used in this study contain three tandem copies. Human influenza hemagglutinin (HA)-tagged Plk4 constructs containing the full-length (pKM3855), C (pKM3671), CPB_L (pKM3862), CPB_{M1} (pKM3886), CPB_{M2} (pKM3885), CPB (pKM3672), PB1 (pKM4339), PB2 (pKM4340), or PB3 (pKM3673) of Plk4 were cloned into the pCI-neo-HA vector in the same way as described above.

To construct full-length FLAG-Plk4 mutants, a respective *Pme*I-*Not*I fragment containing a K608A (pKM4447), K625A (pKM4441), K634A (pKM4442), K681A (pKM4443), R684A (pKM4414), K685A (pKM4448), or K711A (pKM4444) mutation was inserted into the CI-neo-FLAG vector digested by the same enzymes.

The pEGFP-C1-Cep192 (pKM3552) construct expressing the full-length Cep192 (residues 1–2538) and pEGFP-C1-Cep152 (pKM3841) expressing the full-length Cep152 (residues 1–1654) are described previously [3]. To generate pCI-neo-FLAG-Cep192Δ58 (pKM4719) lacking residues 201–258, the N-terminus of pCI-neo-FLAG-Cep192 (pKM4199) construct [3] was replaced with a Cep192Δ58 fragment digested by *Asc*I and *Bcl*I. The pEGFP-C1-Cep152 (E21K) (pKM4100) construct was generated by inserting a *Xho*I-*Sma*I fragment into the pEGFP-C1 vector digested by the corresponding enzymes.

To construct GFP fusion protein of Cep192 (201–280) (pKM3512) or Cep152 (1–217) (pKM3561), a *Sal*I-*Sma*I fragment was inserted into the pEGFP-C1 vector digested by the same enzymes.

To generate serially deleted constructs from pEGFP-C1-Cep152 (1–217) (pKM3561), a *Sal*I-*Sma*I fragment containing Cep152 (1–200) (pKM3800), Cep152 (1–175) (pKM3801), Cep152 (1–150) (pKM3802), Cep152 (1–130) (pKM3803), Cep152 (1–110) (pKM3804), Cep152 (1–100) (pKM3835), Cep152 (1–90) (pKM3836), Cep152 (1–80) (pKM3837), Cep152 (1–68) (pKM3838), Cep152 (1–60) (pKM3839), Cep152 (1–50) (pKM3840), Cep152 (10–217) (pKM3805), or Cep152 (37–217) (pKM3806) was cloned into the pEGFP-C1 vector digested by the respective enzymes.

To create a FLAG-tagged Cep135 (pKM4419) construct, a *Sma*I-*Xho*I fragment from pcDNA3.1-HA-Cep135 (a gift of by Kunsoo Rhee, Seoul National University, South Korea) was subcloned into the pCI-neo-FLAG vector digested by *Pme*I and *Xho*I.

For the lentiviral constructs expressing siRNA-insensitive *CEP152-sil* WT (pKM4325), *CEP152-sil (V8A)* (pKM4329), or *CEP152-sil (E21K)* (pKM4330), a *Xho*I (end-filled)-*Sma*I fragment containing *CEP152-sil* WT or the corresponding mutant was inserted into a pHR′.J-CMV-SV-puro vector (pKM2994) digested by *Sma*I.

To generate bacterial expression constructs, an *Nde*I-*Xho*I fragment containing Plk4 CPB (pKM3677), Cep192-58mer (201–258) (pKM4371), Cep152-60mer (1–60) (pKM4276), Cep192 (201–280) (pKM3544), or Cep152 (1–217) (pKM4268) was cloned into the $pHis_6$-MBP-TEV vector [11] digested by the corresponding enzymes. To generate $pHis_6$-MBP-TEV-Cep192 full-length (pKM4595) and $pHis_6$-MBP-TEV-Cep152 full-length (pKM4596), an *Nde*I-*Sal*I fragment of Cep192 and an *Nde*I-*Xho*I fragment of Cep152, respectively, were cloned into a $pHis_6$-MBP-TEV vector digested by *Nde*I and *Xho*I. To express MBP_L (a longer form of MBP with a 30 residue insertion)-fused Cep192-58mer, a *Eco*RI-*Sal*I fragment containing the MBP C-terminal 30 residue-TEV-Cep192-58mer from pKM4371 was cloned into the pMAL-C2 vector (New England Biolabs) digested by the same enzymes. MBP_L-fused Cep192-58mer migrates markedly slower than MBP-fused Cep152-60mer, thus allowing us to differentiate these two proteins in SDS-PAGE. pGEX-4T3-Plk4 C (580–970) (pKM3584) was cloned by inserting a *Sal*I-*Not*I fragment into the pGEX-4T3 vector (Amersham Pharmacia) digested by the same enzymes. pET21b-Cep192 (201–310) (pKM3619) was generated by inserting a *Not*I-*Sal*I fragment into the pET21b vector (Novagen) digested by the corresponding enzymes. To generate bacterial constructs expressing either His_6-Cep192 (2240–2538) (pKM4251) or GST-Cep192 (2240–2538) (pKM3944), a *Sal*I-*Not*I fragment containing the corresponding Cep192 coding sequence was cloned into the pET21b or the pGEX-4T3 (Pharmacia) vector digested by the same enzymes, respectively.

Supplementary References

1 Johmura, Y. *et al.* Regulation of microtubule-based microtubule nucleation by mammalian polo-like kinase 1. *Proc. Natl. Acad. Sci. USA*. **108**, 11446-11451. (2011).

2 Leung, G. C. *et al.* The Sak polo-box comprises a structural domain sufficient for mitotic subcellular localization. *Nat. Struct. Biol.* **9**, 719-724. (2002).

3 Kim, T.-S. *et al.* Hierarchical recruitment of Plk4 and regulation of centriole biogenesis by two centrosomal scaffolds, Cep192 and Cep152. *Proc. Natl. Acad. Sci. USA*. 110:E4849-4857 (2013).

4 Emsley, P. & Cowtan, K. Coot: model-building tools for molecular graphics. *Acta Crystallogr. D Biol. Crystallogr.* **60**, 2126-2132. (2004).

5 Larkin, M. A. *et al.* Clustal W and Clustal X version 2.0. *Bioinformatics.* **23**, 2947-2948. (2007).

6 Yun, S. M. *et al.* Structural and functional analyses of minimal phosphopeptides targeting the polo-box domain of polo-like kinase 1. *Nat. Struct. Mol. Biol.* **16**, 876-882. (2009).

7 Sillibourne, J. E. *et al.* Autophosphorylation of polo-like kinase 4 and its role in centriole duplication. *Mol. Biol. Cell* **21**, 547-561. (2010).

8 Elbashir, S. M. *et al.* Duplexes of 21-nucleotide RNAs mediate RNA interference in cultured mammalian cells. *Nature* **411**, 494-498. (2001).

9 Cizmecioglu, O. *et al.* Cep152 acts as a scaffold for recruitment of Plk4 and CPAP to the centrosome. *J. Cell Biol.* **191**, 731-739. (2010).

10 Zhao, H. *et al.* The Cep63 paralogue Deup1 enables massive de novo centriole biogenesis for vertebrate multiciliogenesis. *Nat Cell Biol.* **15**, 1434-1444. (2013).

11 Elia, A. E. *et al.* The molecular basis for phospho-dependent substrate targeting and regulation of Plks by the polo-box domain. *Cell* **115**, 83-95. (2003).